Characterization of unsaturated porous media by high-field and low-field NMR relaxometry

L. R. Stingaciu,[1] A. Pohlmeier,[1] P. Blümler,[2] L. Weihermüller,[1] D. van Dusschoten,[2] S. Stapf,[3] and H. Vereecken[1]

Received 16 September 2008; revised 10 March 2009; accepted 29 May 2009; published 11 August 2009.

[1] A comparison study of nuclear magnetic resonance relaxometry at high and low magnetic field (7 and 0.1 T) has been initiated for investigating the influence of the magnetic field strength, variable clay content, and different degrees of saturation on the relaxometric properties of four ideal porous media. The samples consisted of medium sand with increasing fractions of kaolin clay ranging from 0 to 15%. Six different volumetric water contents between saturation and $\theta = 0.05$ were used. Changes in water content of the samples were achieved by slow evaporation. T_2 relaxation curves were monitored by the Carr-Purcell-Meiboom-Gill sequence and were further analyzed by inverse Laplace transformation, yielding T_2 distribution functions. Sand shows a slight continuous shift with decreasing water content of a bimodal distribution function of T_2 to faster relaxation at high and low magnetic field. Sand-clay mixtures show broad, bimodal distribution functions for both magnetic field intensities which shift slightly with decreasing water content. Signal amplitude behavior with variation of saturation degree was also monitored. An expected proportionality of the total signal amplitude with water content was observed for all samples at 0.1 T, whereas at 7 T deviations occurred for samples with a clay content higher than 5%, which are assigned to loss of signal in the first echo periods. The relaxivity in unsaturated clay-based porous media is mostly surface dominated, as the weak and comparable dependence of $1/T_2$ on T_E at both field strengths shows. Nevertheless, for a reliable determination of water content in mixed systems with varying texture and saturation the employment of multiecho sequences at low magnetic field strength are preferable.

Citation: Stingaciu, L. R., A. Pohlmeier, P. Blümler, L. Weihermüller, D. van Dusschoten, S. Stapf, and H. Vereecken (2009), Characterization of unsaturated porous media by high-field and low-field NMR relaxometry, *Water Resour. Res.*, *45*, W08412, doi:10.1029/2008WR007459.

1. Introduction

[2] Nuclear magnetic resonance (NMR) is a noninvasive and nondestructive method that can be used for the characterization of pore spaces in natural porous media. One may differentiate between three ways of application: (1) NMR imaging (magnetic resonance imaging (MRI)) allows for spatial detection of water contents and tracer transport [e.g., *Herrmann et al.*, 2002; *Pohlmeier et al.*, 2009], (2) NMR diffusometry determines the self-diffusion of the water molecules [*Vogt et al.*, 2002], and (3) NMR relaxometry (NMRR) determines magnetic properties of water such as longitudinal and transverse relaxation times in natural porous media [*Kleinberg*, 1996]. These quantities are closely related to intrinsic properties of the pore spaces and their degree of saturation.

[3] With respect to imaging, NMR relaxometry forms the basis of understanding signal intensities and contrast since MRI signal intensities depend on local water content and relaxation times in the respective samples. So, in order to measure spatial water distributions one should first investigate the relaxometric properties of the porous media of interest. Over the last years new NMR methodologies and applications were developed and tested to quantify the total amounts of fluid phase, fluid saturation, and porosity distributions in porous media [*Kleinberg and Horsfield*, 1990; *Latour et al.*, 1995; *Hinedi et al.*, 1997; *Schaumann et al.*, 2005; *Ioannidis et al.*, 2006; *Gladkikh et al.*, 2007]. However, the majority of works on NMR relaxometry in natural porous media have been performed on consolidated porous materials such as rocks [*Hedberg et al.*, 1993; *Kleinberg*, 1994; *Straley et al.*, 1997] because of their importance for oil well logging applications. In general, the amplitude of the ^{1}H NMR relaxation curve provides information about the fluid content of the rocks, while the transversal relaxation times are used for the characterization of the pore size distribution [*Dunn et al.*, 2002]. NMR relaxometry has also proved to be a convenient tool for the characterization of water in soils. *Amin et al.* [1996], *Hall et al.* [1997], and *Votrubová et al.* [2000] investigated the relationship between known water content in the samples and the amount of water detected by MRI employing different NMR pro-

[1] Agrosphere Institute, Forschungszentrum Jülich, Jülich, Germany.
[2] Phytosphere Institute, Forschungszentrum Jülich, Jülich, Germany.
[3] Department of Technical Physics II, University of Technology, Ilmenau, Germany.

0043-1397/09/2008WR007459

tocols. Because of the fact that many soils are characterized by quite fast transversal relaxation times they recommended the usage of low-field NMR for the characterization of natural soils, since T_2 should increase with decreasing field strength.

[4] On the other hand, echo intensities depend not only on the water content θ, but also on relaxation times and experimental parameters such as echo time, T_E, and repetition times. Therefore, *Edzes et al.* [1998] proposed to use multiecho NMR sequences for more reliable water content determination. Here, several echoes are recorded for each point in space, and convenient relaxation functions are fitted to the data yielding amplitude and T_2 maps of the sample. The amplitude maps contain only information about the water content, and the influence of the samples texture is contained in the relaxation time maps.

[5] The detection of NMR signal in natural soils can be seriously reduced by acceleration of the relaxation processes due to the presence of paramagnetic impurities such as Fe^{3+} and Mn^{2+} ions [*Hall et al.*, 1997; *Keating and Knight*, 2007]. For certain conditions, such as very high concentrations of paramagnetic ions or excessive internal magnetic field gradients, the signal lifetime might be on the order or below the instrumental receiver dead time. Furthermore, the decrease of water content may also accelerate the relaxation because of the decreasing fluid volume at constant solid-liquid interface area leading to enhanced contribution of the surface relaxivity to the overall transverse relaxation. Especially for low water contents a direct influence of the vapor phase on relaxation in the adsorption layer was demonstrated by *Mattea et al.* [2004].

[6] At all solid-liquid interfaces magnetic susceptibility differences cause local magnetic field gradients, gradients that only influence the transversal relaxation process and thus lead to additional relaxation and hence reduced signal intensity due to diffusion of water in these gradients. Since the magnitudes of these effects depend on the strength of the main magnetic field B_0, they should diminish with decreasing magnetic field strength. Most conventional scanners operate at high field but prior knowledge suggests the usage of low-field scanners, which are currently under development for soil science purposes [*Raich and Blümler*, 2004].

[7] The objective of our work is a comparison study of NMR relaxometric behavior of porous model systems at high and low magnetic field in order to assess the effect of magnetic field strength on transversal relaxation time and signal amplitude at different degrees of saturation. As model systems four mixtures of medium sand and variable fraction of kaolin clay were used, whose relaxometric properties are investigated at a 300 MHz (7 T) high field and a 4.2 MHz (0.1 T) low-field scanner.

2. NMR Basics

[8] In this section only the basics of NMR relaxivity will be presented, detailed information are available from several textbooks [e.g., *Callaghan*, 1991; *Blümich*, 2000]. NMR is a phenomenon which occurs when atomic nuclei with finite spin (e.g., ^{1}H, spin = 1/2) are immersed in a static magnetic field B_0 and exposed to a second oscillating magnetic field B_1 (J. P. Hornak, Basics of NMR, 1997, available at http://www.cis.rit.edu/htbooks/nmr/bnmr.htm). In practice, the unpaired nuclear spins of the ^{1}H, ^{23}Na, ^{13}C, and ^{19}F nuclei are the most important spins for NMR investigation. When an external magnetic field is applied the spins start to precess about the field direction with the Larmor frequency

$$\omega_0 = \gamma \cdot B_0 \tag{1}$$

where γ is the gyromagnetic ratio (1/T s) and B_0 is the magnetic flux density (T). For systems with spin 1/2 only two states are allowed: (1) precession parallel to B_0 (spin up, lower-energy state) and (2) precessions antiparallel (spin down, higher-energy state). For an ensemble of spins these energy states are populated according to Boltzmann's law and the difference between both populations makes up the net magnetization, M_0. At equilibrium, the net magnetization vector lies along the direction of the applied magnetic field B_0. By exposing the nuclear spin system to an electromagnetic radiation of frequency $\omega_0/2\pi$ it is possible to excite the spins and change the orientation of initial magnetization. After excitation two relaxation processes take place simultaneously: (1) longitudinal relaxation (restoration of thermodynamic equilibrium), which is described by the spin lattice relaxation time T_1, and (2) transversal relaxation (loss of coherence of the detected transverse magnetization), which for a Carr-Purcell-Meiboom-Gill sequence (CPMG) sequence of the nth echo is described by the spin-spin relaxation time T_2:

$$M_{xy}(t) = M_0 \cdot \exp\left(-n \cdot T_E / T_{2app}\right) \tag{2}$$

$$\frac{1}{T_{2,app}} = \frac{1}{T_{2,bulk}} + \frac{1}{T_{2,diff}} + \frac{1}{T_{2,surf}} = \frac{1}{T_{2,bulk}} + \beta T_E^2 + \frac{1}{T_{2,surf}} \tag{3}$$

$$\beta = \frac{D}{12}(\gamma G)^2 \tag{4}$$

where M_{xy} is the transversal magnetization (A/m) in the xy plane perpendicular to the main magnetic field B_0 (T); M_0 is the magnetization immediately after the 90° pulse, which is proportional to the spin density, i.e., the number of ^{1}H atoms in the sample; and T_E is the echo time (s), T_{2app} is the apparent relaxation time (s), $T_{2,diff}$ comprises the diffusion effect, and $T_{2,surf}$ is the surface enhanced transverse relaxation rate. The factor β (s^{-3}) describes diffusion in local internal magnetic field gradients [*Barrie*, 2000]. Finally, D (m^2/s) is the diffusion coefficient of water and G (T/m) is the strength of the magnetic field gradient. The apparent transverse relaxation time can be measured in a single experiment using the CPMG spin echo method resulting in a short measurement time; the true value can then be obtained by employing a sufficiently short echo time that will minimize the diffusion term in equation (3).

[9] In porous media NMR relaxation is accelerated by the collision of excited spins with pore walls. The standard theory for this phenomenon relates the transverse relaxation time with pore dimension [*Barrie*, 2000; *Brownstein and Tarr*, 1977, 1979]

$$\frac{1}{T_2} = \frac{1}{T_{2,bulk}} + \rho_2 \cdot \frac{S}{V} \tag{5}$$

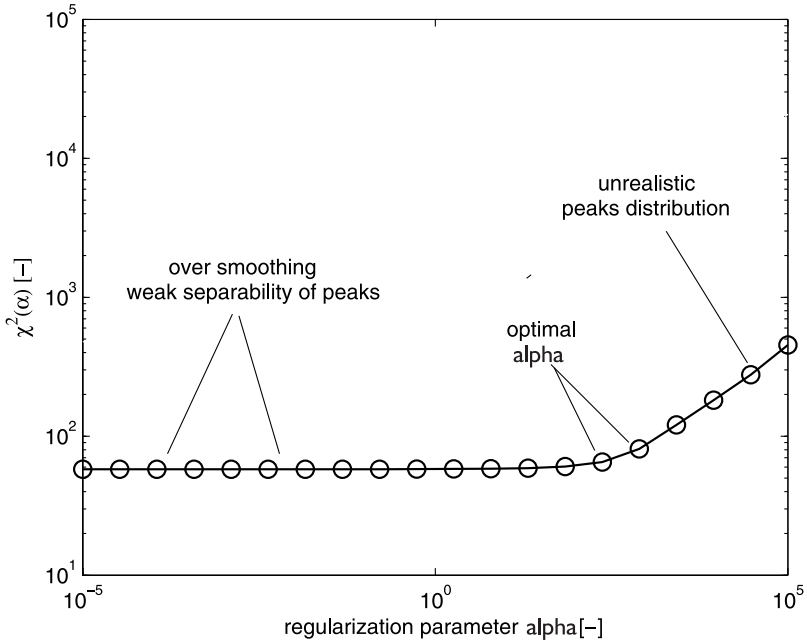

Figure 1. Determination of the regularization parameter α from the variance $\chi^2 = f(\alpha)$. Plot of $\chi^2(\alpha)$ as calculated by equation (8) for the saturated sample Mix15.

where ρ_2 is the surface relaxivity parameter (Å/s) consisting of the properties of the solid-liquid interface and is assumed to be constant for a given sample and S/V is the surface to volume ratio (m^{-1}) which is a measure of the pore size.

[10] As stated above, T_2 is influenced by pore sizes, their distribution, and by the properties of the solid-liquid interfaces. Therefore, a multiexponential decay of the signal is expected in a heterogeneous medium and equation (2) is represented by a Laplace transformation of the distribution function of T_2 relaxation times, F(T_2) [*Song et al.*, 2002],

$$M_{xy}(t) = \int_{T_2\,\min}^{T_2\,\max} \mathcal{F}(T_2)\exp(-n \cdot T_E/T_2)dT_2 + E(t) \qquad (6)$$

Equation (6) can be represented in a discretized matrix form:

$$\mathbf{Y} = \mathbf{KX} + \mathbf{E} \qquad (7)$$

where $\boldsymbol{X}$ is the distribution function to be determined, $\mathbf{Y}$ is the measured signal, $\mathbf{K}$ is the known matrix of the kernel ($\exp(-n \cdot T_E/T_k)$) with T_k as the fixed relaxation times, and $\mathbf{E}$ is the experimental noise. However, the determination of the distribution function by a simple nonnegative least square fit is a mathematically ill-posed problem. To overcome this problem, a so-called regularization function is added to the system of equations. Several regularization procedures have been proposed, whereby the most commonly used one is the second derivative of the distribution function X'' which defines the smoothing amount, controlled by the regularization parameter α. Finally, the regularized variance can be written as

$$\chi^2 = \left\|\mathbf{KX} + \mathbf{E}\right\|^2 + \alpha^{-1}\left\|\mathbf{X}''\right\|^2 \qquad (8)$$

The first right-hand term in equation (8) is the classical least squares fit; the second term is the regularization function. The optimal value of the regularization parameter α is chosen from representation of χ^2 as a function of log α as demonstrated in Figure 1. The distribution function is represented by a semilogarithmic plot of F(T_2) as a function of m logarithmically spaced T_2 values. It is also convenient to calculate the average T_2 relaxation time according to equation (9):

$$\log(T_{2,\mathrm{av}}) = \frac{\sum_{i=1}^{m} A_i \log T_{2i}}{\sum_{i=1}^{m} A_i} \qquad (9)$$

where A_i is signal amplitude (arbitrary units) of the ith function of the discretized distribution function, m is number of the function (here m = 100) and T_{2i} is the corresponding relaxation time (ms).

3. Materials and Methods

3.1. Porous Media

[11] Four samples were prepared from pure sand (FH31, Quarzwerke Frechen, Germany) with a grain size distribution of: 2% (>0.72 mm), 8% (0.71–0.5 mm), 30% (0.5–0.355 mm), 41% (0.36–0.25 mm), 16% (0.25–0.18 mm), 3% (<0.18 mm) mixed with kaolin clay (Sigma-Aldrich, Germany) in a range of 0, 5, 10, and 15 mass percentages. In the following, these samples will be named as FH31, Mix5, Mix10, and Mix15, respectively. The sand-clay mixtures were carefully homogenized (MRI images of thin slices of the samples are presented in Figure 2 and they show homogeneous distribution of the water content in the saturated samples) and filled into glass tubes with an inner diameter of 24 mm and a height of 46 mm. The bottom of

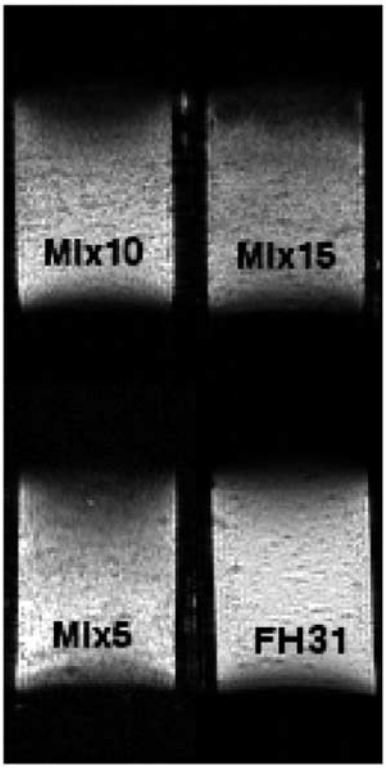

Figure 2. MRI images for the saturated samples recorded at $T_E = 2$ ms and a resolution of 0.23 mm^2 per pixel (field of view 70 × 28 mm).

the tubes consists of a porous glass plate with a pore size between 40 and 90 μm (RoBu, Germany). This allows saturating the system from the bottom which was carried out for all samples with degassed water for 1 day, after which the samples were sealed on both ends. Unsaturated conditions were obtained by removing the seal on the top of the samples to allow evaporation for a certain time and then the seal was replaced. Before measurement, each sealed sample was allowed to equilibrate at room temperature for 1 day. The characteristics for all samples: bulk density (g/cm^3); saturated water content θ_s (cm3/cm^3) and the bulk water content after each evaporation step are summarized in Table 1. The implications of the evaporation procedure stated above on the vertical water content distribution and the corresponding NMR measurements are discussed below.

3.2. NMR Setup

[12] For high-field experiments a 7 T (300 MHz ^{1}H resonance frequency) vertical wide bore superconducting magnet (Oxford Instruments, United Kingdom) connected to a Varian console was used. The NMR RF resonator is a ''birdcage''-type resonator with an internal diameter of 3.8 cm and 7 cm length. The low-field experiments were conducted on a 0.1 T (4.2 MHz ^{1}H resonance frequency) Halbach magnet (ACT, Aachen, Germany) as described by *Raich and Blümler* [2004], connected to a KEA spectrometer (Magritek, New Zeeland). The resonator was a solenoid RF coil of 3.5 cm inner diameter and 5 cm length. The temperature in the laboratories was regulated to 21°C. For the determination of signal amplitude and T_2 relaxation time the CPMG pulse sequence was employed [*Carr and Purcell*, 1954; *Meiboom and Gill*, 1958]. This multiple pulse sequence consists of the application of a 90° RF excitation pulse followed after duration of $T_E/2$ by a series of 180° RF pulses of distance T_E in order to refocus the net magnetization. After the ith 180° pulse, a spin echo is formed of which only the central point is acquired with a delay of $i \cdot T_E$ ($i = 1 \ldots n$) referred to the initial 90° RF pulse.

[13] Parameters used for the high-field measurements are: $T_E = 0.4$ ms (the minimum possible with this setup), number of echoes $n = 10000$, repetition time, $T_R = 6$ s for a number of 2 signal accumulations. For low-field experiments the parameters were: $T_E = 0.2$ ms (the smallest echo times which do not produce truncated information), $n = 12000$ and $T_R = 6$ s for a number of 64 accumulations. The number of acquisition points was in all cases sufficiently high so that the CPMG curves decreased completely into the noise. High-field images of the saturated samples have been recorded with $T_E = 2$ ms and a resolution of 0.23 mm^2 per pixel (128 × 64 pixels for a field of view of 70 × 28 mm).

4. Numerical Simulations

[14] As already stated above, exposing the samples to atmospheric conditions will lead to water loss at the soil surface due to evaporation. In general, evaporation will change the water content distribution within the sample, with lower values at the top end and increasing water contents toward the bottom end. This water content distribution may potentially influence the NMR results. To evaluate the uncertainty in the assumed homogeneity of the sample the water content distribution within the different samples after each evaporation step was analyzed using numerical simulations. Therefore, the software package HYDRUS-1D [*Šimůnek et al.*, 1998] was used which solves numerically Richards' equation for the water flow:

$$\frac{\partial \theta}{\partial t} = \frac{\partial}{\partial z}\left[K(h)\left(\frac{\partial h}{\partial z} - 1\right)\right] \tag{10}$$

Table 1. Characteristic Data of the Samples[a]

Sample	Bulk Density (g/cm^3)	θ_{max} (cm^3/cm^3)	Water Content–Evaporation Steps θ_a (cm^3/cm^3)				
			Step 1	Step 2	Step 3	Step 4	Step 5
FH31	1,69	0.36	0.28	0.26	0.20	0.10	0.05
Mix5	1,57	0.39	0.30	0.26	0.17	0.11	0.06
Mix10	1,59	0.40	0.36	0.26	0.20	0.12	0.09
Mix15	1,60	0.39	0.27	0.19	0.15	0.08	0.05

[a]Shown are bulk density, maximum measured volumetric water content, θ_{max}, and actual mean water contents θ_a for each evaporation step. Note that the water contents were determined gravimetrically.

Table 2. Soil Hydraulic Parameters Used for the Numerical Simulations[a]

Sample	θ_r (cm^3/cm^3)	θ_s (cm^3/cm^3)	α (cm^{-1})	n	K_S (cm/h)	I
FH31	0.0507	0.36	0.0308	4.2464	46.43	0.5
Mix5	0.0565	0.39	0.029	3.2157	24.53	0.5
Mix10	0.0594	0.40	0.029	2.2707	8.83	0.5
Mix15	0.0627	0.39	0.0256	1.7511	3.46	0.5

[a]Here θ_r and θ_s are the residual and saturated water content, respectively, α is the reciprocal value of the air entrance value, n is a shape parameter, K_S is the saturated hydraulic conductivity, and I is the tortuosity. Parameterization according to *van Genuchten* [1980].

where θ is the volumetric water content (cm^3/cm^3), h is the pressure head (cm), z (cm) is the depth, and $K(h)$ is the unsaturated hydraulic conductivity (cm/h). The parameterization of the hydraulic conductivity and water retention is based on the Mualem–van Genuchten approach [*van Genuchten*, 1980], in which the effective volumetric water content S_e is given by

$$S_e = \frac{\theta - \theta_r}{\theta_s - \theta_r} \begin{cases} 1 & h \geq 0 \\ (1 + |\alpha h|^n)^{-m} & h < 0,\ \alpha, m > 0 \quad n > 1 \end{cases} \tag{11}$$

where θ_r (cm^3/cm^3), and θ_s (cm^3/cm^3) are the residual and saturated volumetric water contents, respectively, and α (cm^{-1}), n (−), and m (−) ($m = 1-1/n$) are the shape parameters. Assuming that the tortuosity factor equals 0.5 [*Mualem*, 1976] the Mualem–van Genuchten approach leads to

$$K_r(\psi) = K_s \frac{[1 - (\alpha h)^{mn}\{1 + (\alpha h)^n\}^{-m}]^2}{[1 + (\alpha h)^n]^{\frac{m}{2}}} \tag{12}$$

where K_r is the relative and K_S is the saturated hydraulic conductivity. The hydraulic properties for the sand-clay mixture were estimated using the program Rosetta [*Schaap et al.*, 2001] and are listed in Table 2. The effect of evaporation on the soil water content distribution was simulated for a soil profile of 46 mm nonequidistantly discretized with 300 nodes. The system was initialized in pressure head $h = 0$ (full saturation). The upper boundary was set to variable flux which represents the actual evaporation rate over time calculated from mass (water) loss of each substrate between two consecutive evaporation steps. The evaporation steps and the bulk water loss of the laboratory experiment are listed in Table 1.

5. Results and Discussion

5.1. Relaxation Behavior of Saturated Systems

[15] Figure 2 shows MRI images of the investigated samples. Displayed is the central part (50 × 28 mm) of the columns; the concave curvatures of the upper and lower boundaries are due to the limit of the Rf field. However, the following relaxometric investigations are also performed within these boundaries, so the images represent the investigated volume of the samples. From Figure 2 it is clear that the heterogeneity is in all cases quite similar, the medium sand and the mixtures look identical, no large-scale separation of clay and sand is observed. However, some microscopic heterogeneity remains, especially some air inclusions appear, and the signal intensity varies to about ±3%. So we can conclude that the following relaxometric investigations average over these millimeter-scale inhomogeneities.

[16] Figure 3 shows four exemplary CPMG relaxation curves of saturated samples FH31, Mix5, Mix10 and Mix15, measured in high and low field (with $T_E = 0.4$ ms for $B_0 = 7$ T and $T_E = 0.2$ ms for $B_0 = 0.1$ T). Generally, the

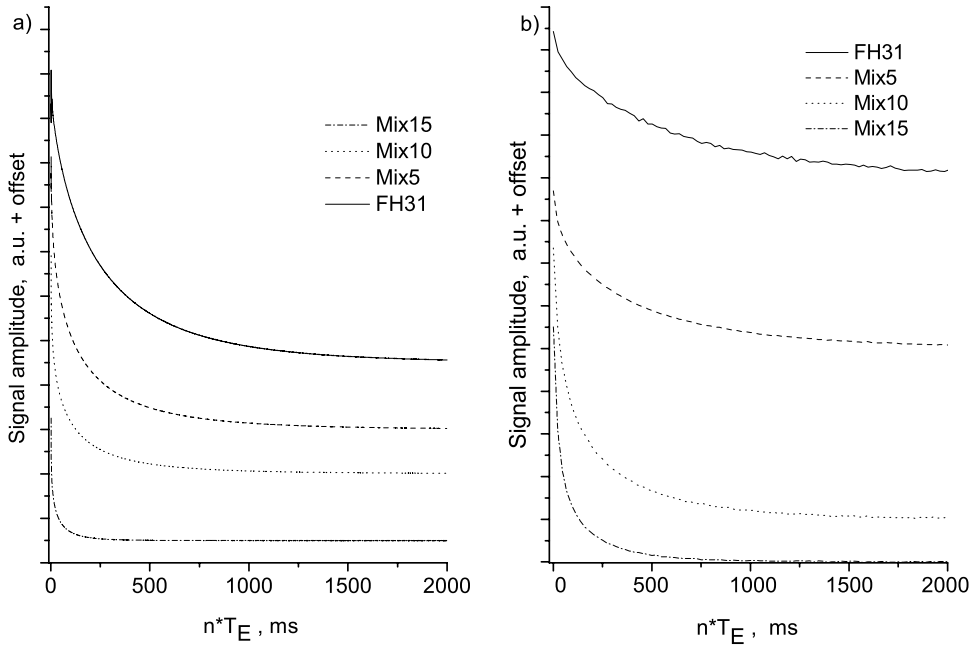

Figure 3. CPMG relaxation curves for all saturated samples at (a) high field, $B_0 = 7$ T (300 MHz) and $T_E = 0.4$ ms, and (b) low field, $B_0 = 0.1$ T (4.2 MHz) and $T_E = 0.2$ ms. For better inspection the curves are offset along the ordinate.

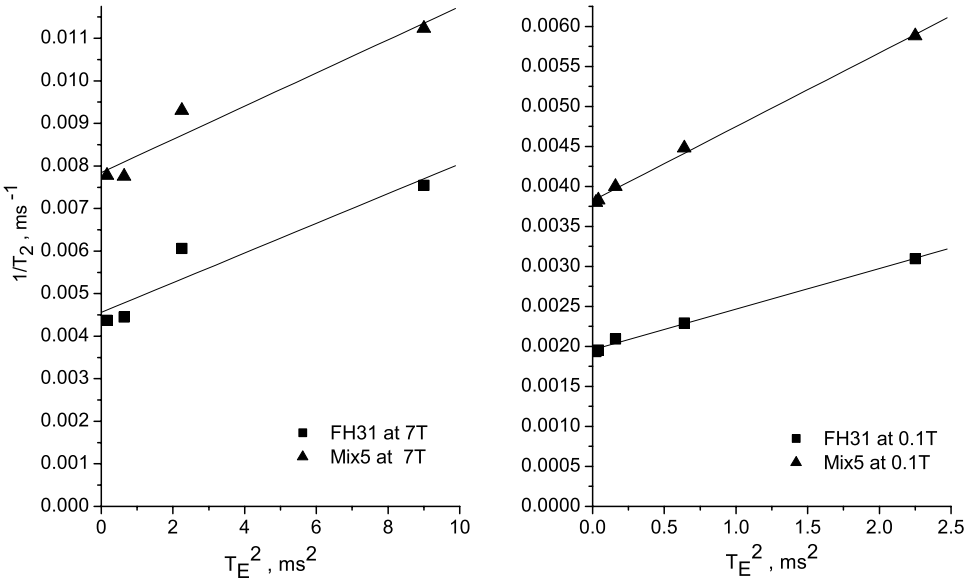

Figure 4. Estimation of diffusion influence: $1/T_{2,\text{average}}$ as a function of T_E^2 at 0.1 and 7 T for two samples, FH31 saturated and Mix5 saturated. The field gradients were estimated using equation (4) to be 1.28 T/m for FH31 and 1.78 T/m for Mix5 in low magnetic field and 1.089 T/m for FH31 and 1.13 T/m for Mix5 in high magnetic field.

relaxation curves decay faster with increasing clay content at both field strengths. The most obvious difference is that at low field the relaxation decays are slower compared to high field. In order to check if the decay of the curves might be additionally affected by diffusion in magnetic field gradients according to equation (3), the influence of T_E on the apparent average T_2 obtained from equation (9) was tested at high and low field.

[17] Figure 4 shows that for saturated FH31 as well as for Mix5 the expected behavior described with equation (3) is observed, indicating that diffusion in internal magnetic field gradients accelerates T_2 relaxation at higher values of T_E. Nevertheless, for lower values of T_E (0.15 ms and 0.2 ms in low field and 0.4 ms in high field) the variations in T_2 are insignificant. Therefore, T_E was set to 0.2 ms (the smallest echo times which do not produce truncated information) for low-field measurements and 0.4 ms in high-field measurements, assuming that $1/T_2$ data obtained with this setting are very close to those obtained with $T_E = 0$ so that the influence of diffusion in residual field gradients is minimal

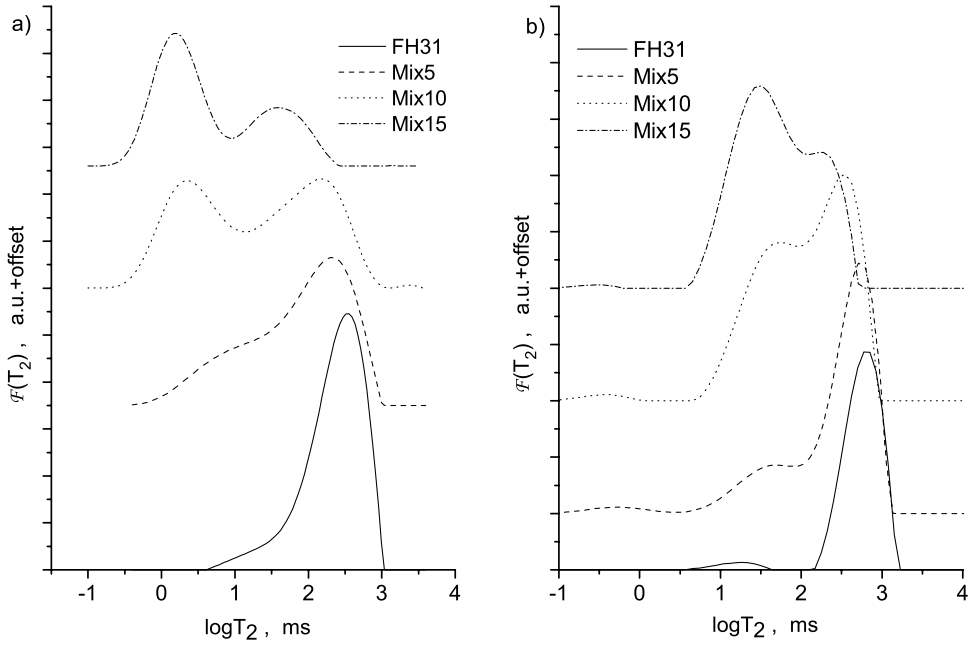

Figure 5. Distribution function $F(T_2)$ for saturated samples at (a) $B_0 = 7$ T and (b) $B_0 = 0.1$ T. Note that data were fitted according to equation (6) using 100 exponentially spaced T_2 values.

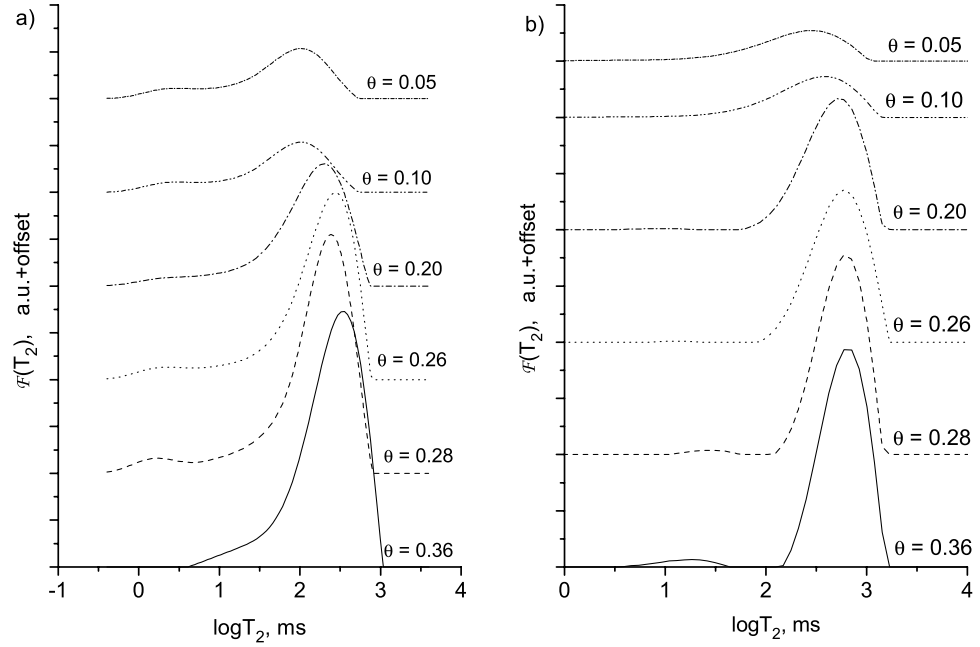

Figure 6. Distribution function $F(T_2)$ for sample FH31 at different water contents: (a) $B_0 = 7$ T and (b) $B_0 = 0.1$ T. Note that data were fitted according to equation (6) using 100 exponentially spaced T_2 values.

and can be neglected for further evaluation. This is in agreement with those of *Keating and Knight* [2007], who found no significant contribution of diffusional relaxation rates for several fine sands. It should be noted that with decreasing water content larger deviations occur.

[18] All curves were analyzed using inverse Laplace transformation according to equation (6). Figure 5 shows the relaxation time distribution functions as obtained by inverse Laplace transformation of the curves in Figure 3 using the program of *Song et al.* [2002]. At both fields strengths bimodal distributions are observed for FH31 and all sand-clay mixtures although the fast mode is hardly resolved for FH31 and Mix5. Nevertheless, these patterns allow one to distinguish between a slow mode at about 300 ms and a fast mode at about 20 ms for FH31 at 7T (300 MHz, Figure 5a). With increasing clay content the fast mode becomes more pronounced and both modes will be accelerated. The explanation for this pattern is the reduction of the pore sizes as a consequence of adding clay to the sand. The bimodality at higher clay contents reflects most probably the existence of clay aggregates (relaxation time around 30 ms) beneath larger pores like in pure sand; that is, the clay tends to aggregate around the sand grains resulting in the redistribution of pores size classes. A complete filling of the pores has not been observed, since the slow mode principally persists. The fact that the overall maximum water content (θ_{max}, Table 2) does not decrease with increasing clay content, but in contrary slightly increases supports this interpretation, that the clay particles do not fill the present pores.

[19] At 0.1 T (4.2 MHz, Figure 5b), FH31 is characterized by a dominant slow mode at 550 ms and a small, fast mode at 15 ms, which contributes less then 2% to the total area. Bimodal behavior is observed for all clay mixtures; however, both modes overlap significantly and are not as well resolved as for high field. Again the relaxation times are shifted, for instance for Mix15 the peaks are shifted to 200 ms (slow mode) and 30 ms (fast mode). The same trend is observed as at high field, with an increase of the fast modes on the expense of the slow ones.

5.2. Relaxivity as a Function of Water Content

[20] One of the main motivations of this research is the detection of the dependence of the relaxation parameters on the water content in different magnetic field strengths. Therefore, the measurements were repeated for all samples at different degrees of water saturation. Figure 6 shows the obtained distribution functions at 7 T and 0.1 T for FH31 at different water contents, θ. For high field (Figure 6a), the distribution is relatively broad and has a bimodal trend with unresolved peaks (shoulder) for higher water contents which broadens with decreasing saturation. It should be noted that the broadening of the distribution with decreasing saturation can also be an effect of the regularization procedure since the first term of the regularization condition is increased by the noise level and the loss of signal amplitude due to the loss of water leads to a smaller signal-to-noise ratio. The total area of the distribution function is also decreasing because of the increasing desaturation. The mean relaxation time shifts from 300 ms at highest water contents to 30 ms for the lowest. For low field (Figure 6b), the distribution functions of FH31 are bimodal with a negligible contribution of a fast mode. This trend is observed only for higher saturations. The relaxation accelerates from $T_{2,average} = 550$ ms to 250 ms with decreasing water contents ranging from $\theta = 0.36$ to 0.05 cm^3/cm^3. The distribution functions for Mix5 are bimodal (Figure 7) in both magnetic fields. With decreasing water saturation the slow and fast mode decreases by a factor of 2 at both field strengths. It is obvious that the contribution of the fast mode increases at the expense of the slow mode. This pattern can be explained by the water retention of the porous material where the water

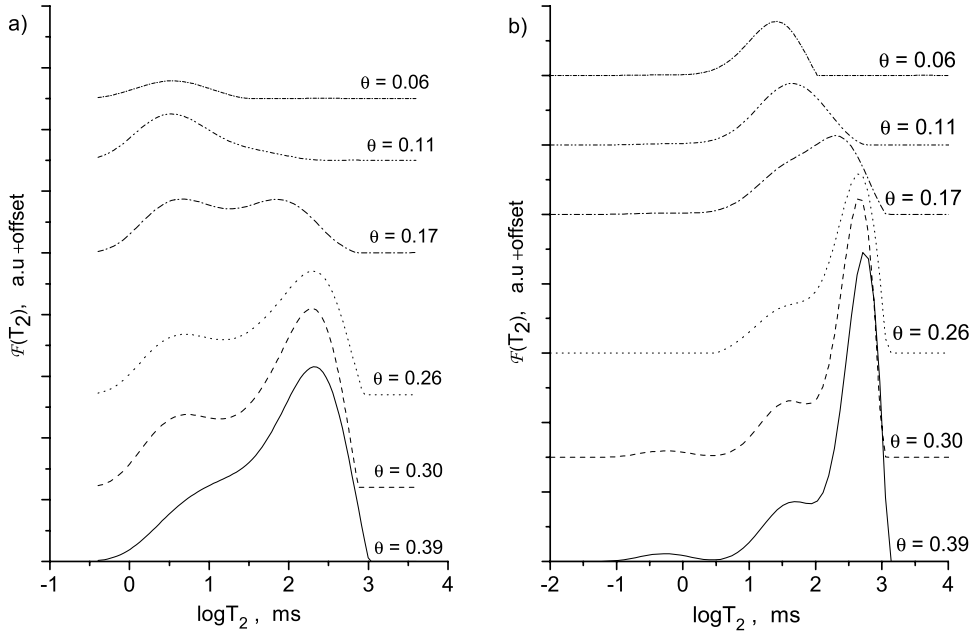

Figure 7. Distribution function $F(T_2)$ for sample Mix5 at different water contents: (a) $B_0 = 7$ T and (b) $B_0 = 0.1$ T. Note that data were fitted according to equation (6) using 100 exponentially spaced T_2 values.

loss will begin in the largest pores and successively smaller pores will be desaturated. Finally, water will remain in the finest pores only. This results in more frequent wall collisions and therefore shorter relaxation times. As a consequence, at very low water content only the fast mode remains. *Bird et al.* [2005] attributes those effects also to a redistribution of water within the soil due to entrapped air within smaller intra-aggregate pores. However, this effect should be taken into account only for very low saturations since at higher saturation the evaporation model shows an even distribution of the water within the sample. This trend is reproducible for all clay mixtures (results not shown).

[21] The remaining question is to what extent the extrapolated signal amplitude is proportional to the water content as suggested by equation (2). The total signal amplitudes for all samples in high and low field are displayed in Figure 8 as function of the water content. In general, at high field (Figure 8a) the relation shows a stronger scattering and clear dependence on the clay content for all samples. With increasing clay content the deviation from proportionality is more pronounced. One possible explanation for this nonlinearity between signal amplitude and integral water content, which was determined gravimetrically, can be the nonuniformity of the water content within the sample due

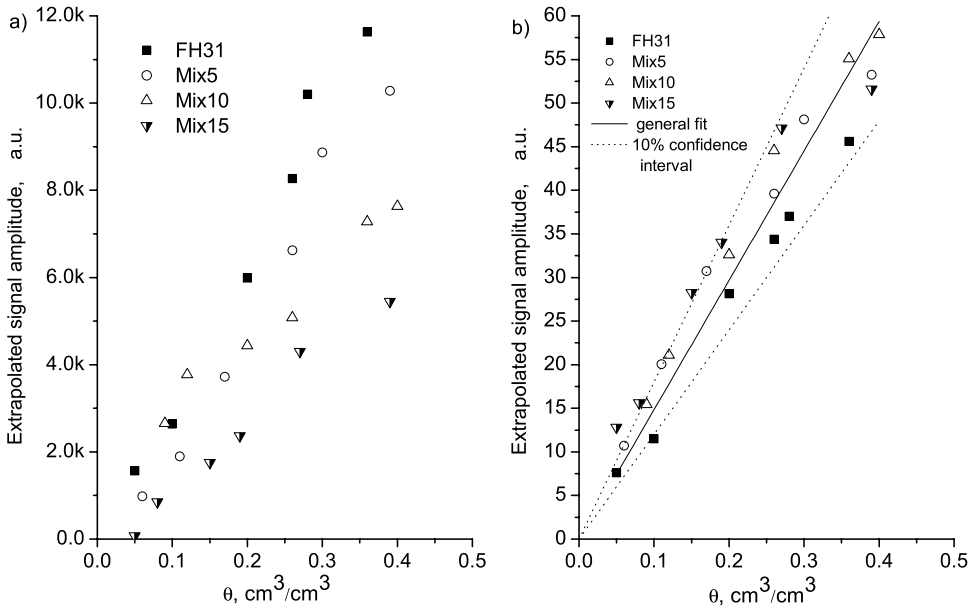

Figure 8. Extrapolated signal amplitudes at different mean volumetric water contents for all samples: (a) $B_0 = 7$ T and (b) $B_0 = 0.1$ T.

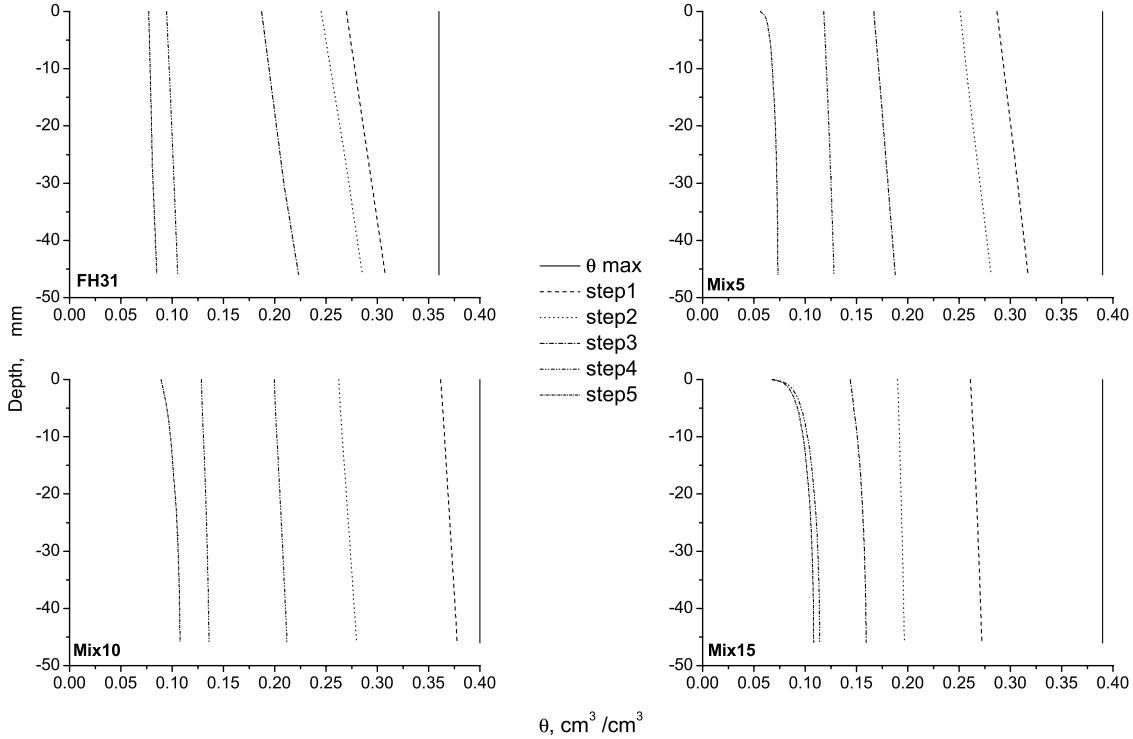

Figure 9. Hydrus-1D model results for the actual water content (cm^3/cm^3) with depth after five evaporation steps for all samples. The soil surface is at depth = 0.

to evaporation at the surface. To check this hypothesis numerical simulations have been performed to check whether large water content gradients will occur during evaporation. Therefore, the simulations were carried out analogously to the sample preparation. The corresponding actual water contents for the four samples over depth are plotted in Figure 9. From these results one may conclude that the water content does not change much with depth for each evaporation step. Only the final step, with smallest water content indicates a steep decline close to the soil surface which is most intense for the mixture with the largest clay fraction (Mix15). A further reason for the observed nonlinearity between signal amplitude and the water content might be the loss of signal during the first T_E period, which is 0.4 ms at high field; that is, fast relaxing components are present, see also Figure 7a. Shorter echo times were technically not possible, so this effect could not be corrected for with the fitting procedure. The consequence is a CPMG echo train amplitude close to zero at nonzero water content, in other words, a part of the water present in the Mix15 sample at $\theta = 0.05$ relaxes faster than about 1 ms.

[22] In contrast to the results at high field, the measurements at low field show a clear linear relation between the extrapolated signal amplitude and the water contents for all samples (Figure 8b). The observed relation has been quantified for all sampled values using linear regression with $M = c \cdot \theta$ with c as the slope and M as signal amplitude resulting in a coefficient of determination of $R^2 = 0.91$. Because these values were determined by extrapolation to time = 0 it is difficult to obtain a realistic error for them. Therefore, the quality of the experiment was estimated using a 10% confidence interval as displayed in Figure 8b which contain more then 95% of the measured values. Hence, an error of 10% seems to be a realistic estimate for the determination of water content from low-field NMR measurements. With respect to magnetic resonance imaging (MRI) these results suggest that in principle a single point calibration will be sufficient to determine water content of soil; however the underlying linear relation must first be confirmed for more realistic samples.

6. Summary and Conclusions

[23] We have investigated the transversal relaxivity of water in medium sand and different sand/kaolin mixtures at high (7 T) and low (0.1 T) magnetic fields, by means of the CPMG pulse sequence as a function of water contents and composition. The data were analyzed by inverse Laplace transformation. Before starting the conclusions, the major trends observed at both field strengths are summarized.

[24] 1. The dispersion of the relaxation times, i.e., their dependence on the main magnetic field, is similarly weak, e.g., for medium sand a factor of about 2 is found while the field strength increases by a factor of 70; for Mix5 the slow and fast modes are accelerated by factors of 2 and 5, respectively, while the magnetic field strength increases from 0.1 to 7 T. The acceleration due to internal magnetic field gradients is most probably not the reason for this dispersion since the gradient strengths are comparable (values are presented in the caption of Figure 4).

[25] 2. For pure sand, at 7 T a broad bimodal distribution function was observed. The main mode (≈95% of the amplitude) is accompanied by a broad shoulder at shorter T_2. Both modes shift to faster relaxation with decreasing water content.

[26] 3. For pure sand, at 0.1 T a medium broad (1 order of magnitude) bimodal distribution function was observed. At saturated state a fast mode which contributes less then 2% to the total area is present. With decreasing water content the main mode shifts slightly to faster relaxation while the fast mode remains approximately at constant relaxation time.

[27] 4. For mixtures, at 7 T bimodal broad distribution functions ranging over 3 orders of magnitude have been observed, which shift to shorter relaxation times with increasing content of kaolin by 1 order of magnitude between 5 and 15% kaolin.

[28] 5. For mixtures, at 0.1 T bimodal distributions functions also occur, with a smaller width than at high field. The shift to shorter relaxation times is much less pronounced: a factor of three for the slow mode and no shift of the fast mode.

[29] 6. For absolute amplitudes, at low field all measured amplitudes of the relaxation curve are proportional to the absolute water content. At high field the relation shows a stronger scattering of the extrapolated amplitudes with water contents and their slopes decrease with increasing kaolin content in the sample.

[30] These measurements show conclusively that the transverse relaxation time, T_2, is affected by both the variation of clay content and the variation of water content in the samples. At low magnetic field, by increasing the clay content the dominant effect is an increase of the total signal amplitude and relaxation rate. This phenomenon is strongly related to the porosity of the samples and the pore size distribution. By increasing the clay content in the sample the pore size distribution is shifted toward smaller pore sizes. Since the bulk relaxation rate is not significantly enhanced, the apparent relaxation recorded at sufficiently short echo time so that the diffusion influence can be neglected is best discussed in terms of the surface relaxation according to equation (3). Here ρ_2 is a factor that comprises several properties of the surface: surface concentration of paramagnetic centers, diffusivity at the surface, local magnetic field gradients around these centers, local topology of the surface etc. For natural systems these factors are hard to control, so the most convenient (and most taken) way is to define an average value of ρ_2 in order to derive pore size distributions. However, since this assumption might be invalid, we have omitted a rescaling of the found T_2 distribution functions into S/V distributions.

[31] At high field, some fractions of water located in very fine pores might have relaxed during the first echo period and this information is lost resulting in the decrease of signal amplitude with increasing clay content. With decreasing water content, in both magnetic fields, a shift of the apparent relaxation time to smaller values is observed; this is expected, if the surface term in equation (3) dominates transversal relaxivity: $1/T_2$ scales approximately with S/V which is inverse proportional to the degree of saturation θ.

[32] Summarizing, it can be stated that relaxation in unsaturated clay-based porous media is mostly surface influenced. The water content can be determined by multiecho sampling and extrapolation to amplitudes at $t \rightarrow 0$. For a reliable determination of water content in mixed systems with varying texture and saturation the employment of multiecho sequences at low magnetic field strength are recommended.

[33] **Acknowledgments.** Many thanks to Y. Q. Song (Schlumberger-Doll Research, Connecticut) for giving us access to his software for inverse Laplace transform. The DFG (projects PO 746/2-1 and Transregional Collaborative Research Centre 32) has to be acknowledged for financial support and Norbert Klitzsch and Oliver Mohnke (Applied Geophysics, RWTH Aachen University) for providing access to the low field setup. Finally, the reviewers are acknowledged for their very useful comments that helped greatly with the improvement of our paper.

References

Amin, M. H. G., K. S. Richards, R. J. Chorley, S. J. Gibbs, T. A. Carpenter, and L. D. Hall (1996), Studies of soil-water transport by MRI, *Magn. Resonance Imaging*, *14*, 879–882, doi:10.1016/S0730-725X(96)00171-3.

Barrie, P. J. (2000), Characterization of porous media using NMR methods, *Annu. Rep. NMR Spectrosc.*, *41*, 265–278, doi:10.1016/S0066-4103(00)41011-2.

Bird, N. R. A., A. R. Preston, E. W. Randall, W. R. Whalley, and A. P. Whitmore (2005), Measurement of the size distribution of water-filled pores at different matrix potentials by stray field nuclear magnetic resonance, *Eur. J. Soil Sci.*, *56*, 135–143, doi:10.1111/j.1351-0754.2004.00658.x.

Blümich, B. (2000), *NMR Imaging of Materials*, Oxford Univ. Press, Oxford, U. K.

Brownstein, K. R., and C. E. Tarr (1977), Spin-lattice relaxation in a system governed by diffusion, *J. Magn. Resonance*, *26*, 17–24.

Brownstein, K. R., and C. E. Tarr (1979), Importance of classical diffusion in NMR studies of water in biological cells, *Phys. Rev. A*, *19*, 2446–2453, doi:10.1103/PhysRevA.19.2446.

Callaghan, P. T. (1991), *Principles of Nuclear Magnetic Resonance Microscopy*, Oxford Univ. Press, Oxford, U. K.

Carr, H. Y., and E. M. Purcell (1954), Effects of diffusion on free precession in nuclear magnetic resonance experiments, *Phys. Rev.*, *94*, 630–638, doi:10.1103/PhysRev.94.630.

Dunn, K. J., D. J. Bergman, and G. A. Latorraca (2002), *Nuclear Magnetic Resonance: Petro Physical and Logging Applications*, *Handbk. Geophys. Explor.*, vol. 32, Pergamon, Amsterdam.

Edzes, H. T., D. van Dusschoten, and H. Van As (1998), Quantitative T_2 imaging of plant tissues by means of multi-echo MRI microscopy, *Magn. Resonance Imaging*, *16*, 185–196, doi:10.1016/S0730-725X(97)00274-9.

Gladkikh, M., D. Jacobi, and F. Mendez (2007), Pore geometric modeling for petrophysical interpretation of down hole formation evaluation data, *Water Resour. Res.*, *43*, W12S08, doi:10.1029/2006WR005688.

Hall, L. D., M. H. G. Amin, E. Dougherty, M. Sanda, J. Votrubová, K. S. Richards, R. J. Chorley, and M. Cislerova (1997), MR properties of water in saturated soils and resulting loss of MRI signal in water content detection at 2 tesla, *Geoderma*, *80*, 431–448, doi:10.1016/S0016-7061(97)00065-7.

Hedberg, S. A., R. J. Knight, A. L. MacKay, and K. P. Whittall (1993), The use of nuclear magnetic resonance for studying and detecting hydrocarbon contaminants in porous rocks, *Water Resour. Res.*, *29*, 1163–1170, doi:10.1029/92WR02540.

Herrmann, K. H., A. Pohlmeier, A. Wiese, N. J. Shah, O. Nitzsche, and H. Vereecken (2002), Three-dimensional nickel ion transport through porous media using magnetic resonance imaging, *J. Environ. Qual.*, *31*, 506–514.

Hinedi, Z. R., A. C. Chang, and M. A. Anderson (1997), Quantification of microporosity by nuclear magnetic resonance relaxation of water imbibed in porous media, *Water Resour. Res.*, *33*, 2697–2704, doi:10.1029/97WR02408.

Ioannidis, M. A., I. Chatzis, C. Lemaire, and R. Perunarkilli (2006), Unsaturated hydraulic conductivity from nuclear magnetic resonance measurements, *Water Resour. Res.*, *42*, W07201, doi:10.1029/2006WR004955.

Keating, K., and R. Knight (2007), A laboratory study to determine the effect of iron oxides on proton NMR measurements, *Geophysics*, *72*, E27–E32, doi:10.1190/1.2399445.

Kleinberg, R. L. (1994), Pore size distributions, pore coupling, and transverse relaxation spectra of porous rocks, *Magn. Resonance Imaging*, *12*, 271–274, doi:10.1016/0730-725X(94)91534-2.

Kleinberg, R. L. (1996), Utility of NMR T_2 distributions, connection with capillary pressure, clay effect, and determination of the surface relaxivity parameter ρ_2, *Magn. Resonance Imaging*, *14*, 761–767, doi:10.1016/S0730-725X(96)00161-0.

Kleinberg, R. L., and M. A. Horsfield (1990), Transverse relaxation processes in porous sedimentary rock, *J. Magn. Resonance*, *88*, 9–19.

Latour, L. L., R. L. Kleinberg, P. P. Mitra, and C. H. Sotak (1995), Pore-size distributions and tortuosity in heterogeneous porous media, *J. Magn. Resonance, Ser. A*, *112*, 83–91, doi:10.1006/jmra.1995.1012.

Mattea, C., R. Kimmich, I. Ardelean, S. Wonorahardjo, and G. Farrher (2004), Molecular exchange dynamics in partially filled microscale and nanoscale pores of silica glasses studied by field-cycling nuclear magnetic resonance relaxometry, *J. Chem. Phys.*, *121*, 10,648–10,656, doi:10.1063/1.1808423.

Meiboom, S., and D. Gill (1958), Modified spin-echo method for measuring nuclear relaxation times, *Rev. Sci. Instrum.*, *29*, 688, doi:10.1063/1.1716296.

Mualem, Y. (1976), A new model for predicting the hydraulic conductivity of unsaturated porous media, *Water Resour. Res.*, *12*, 593–622.

Pohlmeier, A., D. van Dusschoten, L. Weihermüller, U. Schurr, and H. Vereecken (2009), Monitoring water fluxes in porous media by magnetic resonance imaging using D_2O as a tracer, *Magn. Resonance Imaging*, *27*, 285–292, doi:10.1016/j.mri.2008.06.007.

Raich, H., and P. Blümler (2004), Design and construction of a dipolar Halbach array with a homogeneous field from identical bar magnets: NMR Mandhalas, *Concepts Magn. Resonance, Part B*, *23*, 16–25, doi:10.1002/cmr.b.20018.

Schaap, M. G., F. J. Leij, and M. T. van Genuchten (2001), Rosetta: A computer program for estimating soil hydraulic parameters with hierarchical pedotransfer functions, *J. Hydrol.*, *251*, 163–176, doi:10.1016/S0022-1694(01)00466-8.

Schaumann, G. E., E. Hobley, J. Hurraß, and W. Rotard (2005), H-NMR relaxometry to monitor wetting and swelling kinetics in high-organic matter soils, *Plant Soil*, *275*, 1–20, doi:10.1007/s11104-005-1708-7.

Šímůnek, J., M. Sejna, and M. T. van Genuchten (1998), The HYDRUS-1D software package for simulating the one-dimensional movement of water, heat, and multiple solutes in variably saturated media, version 2.0, U.S. Salinity Lab., Agric. Res. Serv., Riverside, Calif.

Song, Y. Q., L. Venkataramanan, M. D. Hürlimann, M. Flaum, P. Frulla, and C. Straley (2002), T_1–T_2 Correlation spectra obtained using a fast two-dimensional Laplace inversion, *J. Magn. Resonance*, *154*, 261–268, doi:10.1006/jmre.2001.2474.

Straley, C., D. Rossini, H. Vinegar, P. Tutunjian, and C. Morriss (1997), Core analysis by low-field NMR, *Log Anal.*, *38*, 43–56.

van Genuchten, M. T. (1980), A closed-form equation for predicting the hydraulic conductivity of unsaturated soils, *Soil Sci. Soc. Am. J.*, *44*, 892–898.

Vogt, C., P. Galvosas, N. Klitzsch, and F. Stallmach (2002), Self-diffusion studies of pore fluids in unconsolidated sediments by PFG NMR, *J. Appl. Geophys.*, *50*, 455–467, doi:10.1016/S0926-9851(02)00195-7.

Votrubová, J., M. Šanda, M. Císlerová, M. H. G. Amin, and L. D. Hall (2000), The relationships between MR parameters and the content of water in packed samples of two soils, *Geoderma*, *95*, 267–282, doi:10.1016/S0016-7061(99)00091-9.

P. Blümler and D. van Dusschoten, Phytosphere Institute, Forschungszentrum Jülich, ICG-3, D-52425 Jülich, Germany.

A. Pohlmeier, L. R. Stingaciu, H. Vereecken, and L. Weihermüller, Agrosphere Institute, Forschungszentrum Jülich, ICG-4, D-52425 Jülich, Germany. (l.stingaciu@fz-juelich.de)

S. Stapf, Department of Technical Physics II, University of Technology, D-98684 Ilmenau, Germany.